Bulletin of Faculty of Science, Zagazig University (BFSZU)
e-ISSN: 1110-1555
Volume-2025, Issue-4, pp-27-41
https://bfszu.journals.ekb.eg/journal
Research Paper DOI: **10.21608/bfszu.2025.354155.1469**

==========

Negative Velocity Feedback Control of a Nonlinear Oscillating External Panel

Y. A. Amer [1], A.T. EL-Sayed [2], and M. A. EL-Sayed [3, *]
[1] Department of Mathematics, Faculty of Science, Zagazig University, Zagazig, Egypt;yaser31270@yahoo.com
[2] Department of Basic Science, Modern Academy for Engineering and Technology, Elmokattam, Egypt; ashraftaha211@yahoo.com
[3] Department of Mathematics, High Institute of Computers and Information Systems, Fifth Settlement, Egypt;
*Correspondence: marwaabdelaziz750@yahoo.com

***ABSTRACT*: Aircraft wings, especially during flight, experience vibrations due to various forces. This research focuses on controlling these vibrations using a negative velocity feedback controller. The wing is represented as a stepped cantilever plate, acknowledging its complex shape and movement. The study considers several factors influencing wing vibrations: Axial movement: The wing's movement through the air. Smooth surfaces: Aerodynamic forces acting on the wing. Piezoelectric innervation: The use of piezoelectric materials, which can generate electrical charge in response to mechanical stress and vice-versa, for vibration control. Out-of-plane excitation: Forces acting perpendicular to the wing surface. The research uses a combination of theoretical and computational methods: Perturbation methods: Mathematical techniques to approximate solutions to complex nonlinear systems. MATLAB simulations: Computer simulations to model and analyze the wing's dynamic behavior. Routh-Hurwitz criterion: A mathematical test to determine the stability of a system. The study investigates "primary and 1:1 internal resonance condition," which refer to specific vibration modes of the wing. The goal is to determine how effectively the negative velocity feedback controller can suppress these vibrations and maintain stability. Finally, the research validates the accuracy of the methods used by comparing analytical results with numerical simulations.**

***KEYWORDS:* outer plate; multiple time scale method; NVC; nonlinear vibration control; resonance case; stability; frequency Response.**

Date of Submission: 20-01-2025 Date of acceptance: 18-03-2025

Introduction

Axially moving wings, capable of changing their aspect ratio, present a promising alternative to traditional fixed wings in aviation. Their adaptability allows for optimization across various flight conditions, leading to improvements in low-speed performance, landing, and cruising efficiency [1–3]. This is achieved by adjusting the wing's configuration to best suit each phase of flight. When fully extended, the wing offers the stability and lift-to-drag ratio of a fixed wing, proving advantageous for takeoff, landing, and cruising. Researchers are actively studying the complex dynamics of these wings, often using simplified beam, plate, and shell models to analyze their deployment and retraction behavior [4-7]. These investigations, employing theoretical, numerical, and experimental approaches, focus on understanding and addressing potential challenges related to stability and control, ultimately aiming to enhance the performance of these advanced wing systems. The phenomenon of 1:1 internal resonance, often linked to saturation in dynamical systems, can be exploited for active vibration control. A saturation controller, capitalizing on this resonance, effectively suppresses steady-state vibrations by using a quadratic position coupling term and the system's inherent saturation characteristics [8-9]. Proportional-Derivative controllers combine proportional and derivative actions. The proportional action responds directly to the current error (the difference between the desired and actual values), while the derivative action responds to the rate of change of the error, enabling anticipatory corrections. PD controllers are highly effective in reducing vibrations across various applications, from flexible beams to collocated structures, improving system

stability and performance. Active vibration control systems commonly utilize force actuators powered by external energy sources. These actuators, often placed on flexible components like mounts or supports, enhance vibration absorption. A typical setup involves sensors to detect vibrations, electronic circuits to process feedback and determine the necessary actuation force, and actuators to apply a counteracting force to the main structure. This combined approach effectively broadens the frequency range of vibration absorption [10-13]. Using the specified controller resulted in a substantial 94% reduction in vibrations compared to the uncontrolled system. Efficiency, measured as Ea., significantly improved from 16 for a standard PPF controller to 193 with the time-delayed version. Researchers have investigated various control strategies, including those applied to Hybrid Rayleigh-Van der Pol Duffing oscillators, cantilever beams, vertical conveyors, and systems using magneto strictive actuators, to mitigate vibrations in diverse nonlinear dynamical systems [11-22]. These strategies encompass linear velocity and acceleration feedback control, cubic velocity feedback control, nonlinear saturation control, and positive position feedback control. Studies employing the method of multiple scales have analyzed fundamental, subharmonic, and ultra-harmonic resonances, examining equations of motion and steady-state solutions [22-34]. The nonlinear behavior of a forced and self-excited beam with a positive position feedback controller, subjected to harmonic excitation at its support, has also been explored. This study focuses on suppressing vibrations in an outer plate experiencing simultaneous resonance excitations using an NVC controller. The research examines the controller's effectiveness in reducing or eliminating steady-state vibrations and resonances within the plate. Approximate solutions, derived through perturbation methods, offer insights into parameter motion, stability conditions, and jump phenomena, visually represented through graphical analysis. These analytical findings are consistent with numerical results. The uncontrolled system exhibits steady-state vibrations under harmonic excitation, highlighting the need for an effective control mechanism to mitigate these potentially damaging oscillations. The comparative analysis reveals that the NVC-control approach demonstrates superior performance in eliminating vibrations within the system .

Nomenclature

$x, \dot{x}, \ddot{x}$	Movement, speed, and acceleration of the primary mood of the system, consistently.
$y, \dot{y}, \ddot{y}$	Movement, speed and acceleration of second mood of system respectively.
γ_1, b_1	System damping coefficients of main system respectively.
ω_1, ω_2	The constancy of nature of main system respectively.
f	The extent and frequency of an external excitation force or external forces applied to a scheme.
$\gamma_7, \gamma_8, b_7, b_8$	Nonlinear coefficients of the main system.
α_2, α_4	The quantity of NVC control signal
ε	Minor perturbation constraint

List of Abbreviation

MTST	multiple time scale technique
NVC	Negative velocity Feedback controller
SM	simultaneous resonance
FREs	frequency-response equations
IR	Internal resonance

1. *Closed loop model*

1.1. Classification Dynamics without control.

This section introduces the mathematical model of the outer plate system. The system is simplified and modeled as a two-degree-of-freedom system, as depicted in Figure 1.

$$\ddot{x} + \omega_1^2 x + \varepsilon\gamma_1\dot{x} + \varepsilon^2\gamma_5 x^2 y + \varepsilon^2\gamma_6 x y^2 + \varepsilon\gamma_7 x^3 + \varepsilon\gamma_8 y^3 = \varepsilon f_1 \cos\Omega_1 t \quad (1)$$

$$\ddot{y}+\omega_2{}^2 y+\varepsilon b_1\dot{y}+\varepsilon^2 b_5 y^2 x+\varepsilon^2 b_6 x^2 y+\varepsilon b_7 y^3+\varepsilon b_8 x^3=\varepsilon^2 f_2\cos\Omega_2 t \quad (2)$$

1.2. Structure Dynamics with NVC control.

Simplified models, such as the aircraft structure section shown in Figure 1, are commonly used in engineering to analyze the behavior of outer plate systems. A negative velocity feedback controller can mitigate vibrations induced by external forces. The system's behavior under these conditions, including the effects of the external force and the negative velocity feedback controller, is described by Equations (3-4).

$$\ddot{x}+\omega_1{}^2 x+\varepsilon\gamma_1\dot{x}+\varepsilon^2\gamma_5 x^2 y+\varepsilon^2\gamma_6 xy^2+\varepsilon\gamma_7 x^3+\varepsilon\gamma_8 y^3=\varepsilon f_1\cos\Omega_1 t-\varepsilon\alpha_2\dot{x} \quad (3)$$

$$\ddot{y}+\omega_2{}^2 y+\varepsilon b_1\dot{y}+\varepsilon^2 b_5 y^2 x+\varepsilon^2 b_6 x^2 y+\varepsilon b_7 y^3+\varepsilon b_8 x^3=\varepsilon^2 f_2\cos\Omega_2 t-\varepsilon\alpha_4\dot{y} \quad (4)$$

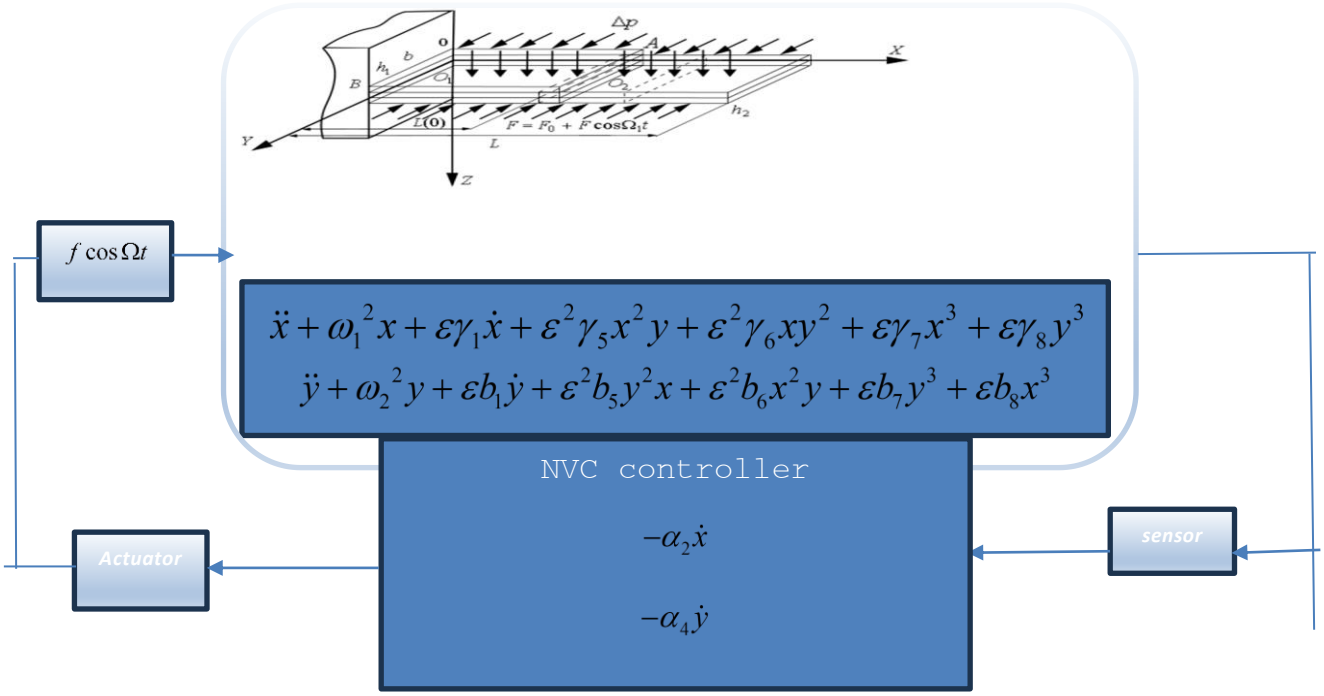

Fig.1: Block chart of outer plate with NVC -controller.

2. *Analytical Investigations*

2.1. Perturbation study

This section employs the method of multiple scales to determine an approximate solution for the nonlinear dynamical system under the proposed NVC controller, leading to a first-order approximation [35-37].

$$\left.\begin{aligned} t &= T_0+T_1+\ldots \\ x(t;\varepsilon) &= x_0(T_0,T_1)+\varepsilon x_1(T_0,T_1)+\mathrm{O}(\varepsilon^2) \\ y(t;\varepsilon) &= y_0(T_0,T_1)+\varepsilon y_1(T_0,T_1)+\mathrm{O}(\varepsilon^2) \end{aligned}\right\} \quad (5)$$

where, the fast scale is T_0 and the slow scale is $T_1=\varepsilon t$. The derivatives using the multiple scales method take the forms:

$$\left.\begin{aligned}\frac{d}{dt}&=D_0+\varepsilon D_1+\varepsilon^2 D_2+\ldots\\ \frac{d^2}{dt^2}&=D_0^2+2\varepsilon D_0 D_1+\ldots\end{aligned}\right\}\quad D_j=\frac{\partial}{\partial T_j}\ (\mathrm{j}=0,1) \tag{6}$$

Inserting equations (5) and (6) in equations (3) & (4) such that:

$$\left(D_0^2+\omega_1^2\right)x_0+\varepsilon\left(D_0^2+\omega_1^2\right)x_1=\varepsilon\begin{pmatrix}-2D_0D_1x_0-\gamma_1D_0x_0-\gamma_7x_0^3-\gamma_8y_0^3\\ -\alpha_2D_0x_0+f\cos(\Omega t)\end{pmatrix}+O(\varepsilon^2) \tag{7}$$

$$\left(D_0^2+\omega_2^2\right)y_0+\varepsilon\left(D_0^2+\omega_2^2\right)y_1=\varepsilon\left(-2D_0D_1y_0-b_1D_0y_0-b_7y_0^3-b_8x_0^3-\alpha_4D_0y_0\right)+O(\varepsilon^2) \tag{8}$$

Equating the coefficients of the same power of ε:

$O(\varepsilon^0)$

$$(D_0^2+\omega_1^2)x_0=0 \tag{9}$$

$$\left(D_0^2+\omega_2^2\right)y_0=0 \tag{10}$$

$O(\varepsilon)$

$$\left(D_0^2+\omega_1^2\right)x_1=-2D_0D_1x_0-\gamma_1D_0x_0-\gamma_7x_0^3-\gamma_8y_0^3-\alpha_2D_0x_0+f\cos(\Omega t) \tag{11}$$

$$\left(D_0^2+\omega_2^2\right)y_1=-2D_0D_1y_0-b_1D_0y_0-b_7y_0^3-b_8x_0^3-\alpha_4D_0y_0 \tag{12}$$

From eq. (9) & (10) Solving the homogenous differential equations we get:

$$x_0(\mathrm{T}_0,\mathrm{T}_1)=A(\mathrm{T}_1)e^{i\omega_1T_0}+\bar{A}(\mathrm{T}_1)e^{-i\omega_1T_0} \tag{13}$$

$$y_0(\mathrm{T}_0,\mathrm{T}_1)=B(\mathrm{T}_1)e^{i\omega_2T_0}+\bar{B}(\mathrm{T}_1)e^{-i\omega_2T_0} \tag{14}$$

Differential equation (13) & (14) with respect to t and submit in equation (11) & (12):

$$\begin{aligned}\left(D_0^2+\omega_1^2\right)x_1=&\left(-2i\omega_1DA-\gamma_1i\omega_1A-3\gamma_7A^2\bar{A}-\alpha_2i\omega_1A\right)e^{i\omega_1T_0}+\\ &f\cos(\Omega t)-3\gamma_8B^2\bar{B}e^{i\omega_2T_0}-\gamma_7A^3e^{3i\omega_1T_0}-\gamma_8B^3e^{3i\omega_2T_0}+CC\end{aligned} \tag{15}$$

$$\begin{aligned}\left(D_0^2+\omega_2^2\right)y_1=&\left(-2i\omega_2DB-b_1i\omega_2B-3b_7B^2\bar{B}-\alpha_4i\omega_2B\right)e^{i\omega_2T_0}\\ &-3b_8A^2\bar{A}e^{i\omega_1T_0}-\gamma_7B^3e^{3i\omega_2T_0}-\gamma_8A^3e^{3i\omega_1T_0}+CC\end{aligned} \tag{16}$$

The complex conjugate parts collected in the term CC. After eliminating the secular terms take the followings forms:

$$\left(-2i\omega_1DA-\gamma_1i\omega_1A-3\gamma_7A^2\bar{A}-\alpha_2i\omega_1A\right)e^{i\omega_1T_0}+f\cos(\Omega t)-3\gamma_8B^2\bar{B}e^{i\omega_2T_0}=0 \tag{17}$$

$$\left(-2i\omega_2DB-b_1i\omega_2B-3b_7B^2\bar{B}-\alpha_4i\omega_2B\right)e^{i\omega_2T_0}-3b_8A^2\bar{A}e^{i\omega_1T_0}=0 \tag{18}$$

From the first approximation, we concluded the following resonance cases: -

i) primary resonance: $\Omega\cong\omega_1$

ii) Internal resonance $\omega_2=\omega_1$

2.2. Episodic resolutions

In this section, the selected manner situation: $\Omega\cong\omega_1,\omega_2\cong\omega_1$ & $\omega_1=\omega_2$ used to deliberate the solubility settings, we will introduce detuning parameters $(\sigma_1)\&(\sigma_2)$ so that:

$$\left.\begin{aligned}\Omega &= \omega_1 + \varepsilon\sigma_1 \\ \omega_2 &= \omega_1 + \varepsilon\sigma_2\end{aligned}\right\} \tag{19}$$

Including equation (19) into the secular and small division terms in equation (17) & (18) for compiling the solvability conditions as:

$$\left(-2i\omega_1 DA - \gamma_1 i\omega_1 A - 3\gamma_7 A^2\bar{A} - \alpha_2 i\omega_1 A\right) + \frac{f}{2}e^{i\sigma_1 T_1} - 3\gamma_8 B^2\bar{B}e^{i\sigma_2 T_1} = 0 \tag{20}$$

$$\left(-2i\omega_2 DB - b_1 i\omega_2 B - 3b_7 B^2\bar{B} - \alpha_4 i\omega_2 B\right) - 3b_8 A^2\bar{A}e^{-i\sigma_2 T_1} = 0 \tag{21}$$

To analyze the solution of (20) and (21) exchanging A and B by the polar form as

$$A(\mathrm{T}) = \frac{1}{2}\mathrm{a}_1(\mathrm{T})\,\mathrm{e}^{i\theta_1 \mathrm{T}_1},, DA(\mathrm{T}) = \frac{1}{2}\left(\dot{\mathrm{a}}_1(\mathrm{T}_1) + ia_1\dot{\theta}_1(\mathrm{T}_1)\right)\mathrm{e}^{i\theta_1 \mathrm{T}_1} \tag{22}$$

$$B(\mathrm{T}) = \frac{1}{2}\mathrm{a}_2(\mathrm{T})\,\mathrm{e}^{i\theta_2(\mathrm{T}_1)},, DB(\mathrm{T}) = \frac{1}{2}\left(\dot{\mathrm{a}}_2(\mathrm{T}_1) + ia_2\dot{\theta}_2(\mathrm{T}_1)\right)\mathrm{e}^{i\theta_2(\mathrm{T}_1)} \tag{23}$$

where a_1 and a_2 This refers to the phases and amplitudes of both the system and the controller when they've reached a stable, unchanging state. In other words, it describes the long-term behavior of their oscillations after any transient effects have died out., and ϕ_1 & ϕ_2 are the phases of the signal. Inserting (22) and (23) into (20) and (21) we get the following amplitude – phase modulating equations:

$$\dot{a}_1 = -\frac{1}{2}\gamma_1\mathrm{a}_1 - \frac{1}{2}\alpha_2\mathrm{a}_1 + \frac{f}{2\omega_1}\sin\phi_1 - \frac{3\gamma_8}{8\omega_1}a_2{}^3\sin\phi_2 \tag{24}$$

$$a_1\dot{\theta}_1 = \frac{3}{8\omega_1}\gamma_7\mathrm{a}_1{}^3 - \frac{f}{2\omega_1}\cos\phi_1 + \frac{3\gamma_8}{8\omega_1}a_2{}^3\cos\phi_2 \tag{25}$$

$$\dot{a}_2 = -\frac{1}{2}b_1\mathrm{a}_2 - \frac{1}{2}\alpha_4\mathrm{a}_2 + \frac{3b_8}{8\omega_2}a_1{}^3\sin\phi_2 \tag{26}$$

$$a_2\dot{\theta}_2 = \frac{3}{8\omega_2}b_7\mathrm{a}_2{}^3 + \frac{3b_8}{8\omega_2}a_1{}^3\cos\phi_2 \tag{27}$$

Where, $\phi_1 = \sigma_1 T_1 - \theta_1$. & $\phi_2 = \sigma_2 T_1 + \theta_2 - \theta_1$ Back to the main system restrictions, we have the following equations:

$$\dot{a}_1 = -\frac{1}{2}\gamma_1\mathrm{a}_1 - \frac{1}{2}\alpha_2\mathrm{a}_1 + \frac{f}{2\omega_1}\sin\phi_1 - \frac{3\gamma_8}{8\omega_1}a_2{}^3\sin\phi_2 \tag{28}$$

$$\mathrm{a}_1\dot{\phi}_1 = \sigma_1\mathrm{a}_1 - \frac{3}{8\omega_1}\gamma_7\mathrm{a}_1{}^3 + \frac{f}{2\omega_1}\cos\phi_1 - \frac{3\gamma_8}{8\omega_1}a_2{}^3\cos\phi_2 \tag{29}$$

$$\dot{a}_2 = -\frac{1}{2}b_1\mathrm{a}_2 - \frac{1}{2}\alpha_4\mathrm{a}_2 + \frac{3b_8}{8\omega_2}a_1{}^3\sin\phi_2 \tag{30}$$

$$a_2\dot{\phi}_2 = (\sigma_2 - \sigma_1)a_2 + a_2\dot{\phi}_1 + \frac{3}{8\omega_2} b_7 a_2^{\,3} + \frac{3b_8}{8\omega_2} a_1^{\,3}\cos\phi_2 \tag{31}$$

2.3. Static opinion answer

Equations (28) through (31) may have an immovable point for a steady-state solution that can be found by putting $\dot{a}_1 = \dot{a}_2 = \dot{\phi}_1 = \dot{\phi}_2 = 0$

$$\frac{f}{2\omega_1}\sin\phi_1 = \frac{1}{2}\gamma_1 a_1 + \frac{1}{2}\alpha_2 a_1 + \frac{3\gamma_8}{8\omega_1} a_2^{\,3}\sin\phi_2 \tag{32}$$

$$\frac{f}{2\omega_1}\cos\phi_1 = \frac{3}{8\omega_1}\gamma_7 a_1^{\,3} - \sigma_1 a_1 + \frac{3\gamma_8}{8\omega_1} a_2^{\,3}\cos\phi_2 \tag{33}$$

$$\frac{3b_8}{8\omega_2} a_1^{\,3}\sin\phi_2 = \frac{1}{2} b_1 a_2 + \frac{1}{2}\alpha_4 a_2 \tag{34}$$

$$\frac{3b_8}{8\omega_2} a_1^{\,3}\cos\phi_2 = (\sigma_1 - \sigma_2)a_2 - \frac{3}{8\omega_2} b_7 a_2^{\,3} \tag{35}$$

Equations (34) and (35) can be squared and then both edges added to become the resulting equation:

$$\left(\frac{1}{2} b_1 a_2 + \frac{1}{2}\alpha_4 a_2\right)^2 + \left((\sigma_1 - \sigma_2)a_2 - \frac{3}{8\omega_2} b_7 a_2^{\,3}\right)^2 = \left(\frac{3b_8}{8\omega_2} a_1^{\,3}\right)^2 \tag{36}$$

Equations (32) and (33) can be squared and then both edges added to become the resulting equation:

$$\begin{aligned}&\left(\frac{1}{2}\gamma_1 a_1 + \frac{1}{2}\alpha_2 a_1 + \frac{3\gamma_8}{8\omega_1} a_2^{\,3}\left(\frac{8\omega_2}{3b_8 a_1^{\,3}}\left(\frac{1}{2} b_1 a_2 + \frac{1}{2}\alpha_4 a_2\right)\right)\right)^2 + \\ &\left(\frac{3}{8\omega_1}\gamma_7 a_1^{\,3} - \sigma_1 a_1 + \frac{3\gamma_8}{8\omega_1} a_2^{\,3}\left(\frac{8\omega_2}{3b_8 a_1^{\,3}}\left((\sigma_1 - \sigma_2)a_2 - \frac{3}{8\omega_2} b_7 a_2^{\,3}\right)\right)\right)^2 = \left(\frac{f}{2\omega_1}\right)^2\end{aligned} \tag{37}$$

Equations and, which describe the system's frequency response, are used to analyze the behavior of the steady-state solutions under typical operating conditions. ($a_1 \neq 0, a_2 \neq 0$).

2.4. Stability examination through linearizing the overhead structure

To determine the stability of the equilibrium solution, the eigenvalues of the Jacobian matrix associated with equations through were analyzed. Asymptotic stability is confirmed if all eigenvalues have negative real parts. Conversely, if any eigenvalue has a positive real part, the equilibrium is unstable. The stability analysis involves examining the behavior of small perturbations around the steady-state solutions $a_{10}, a_{20}, \phi_{10}$ and ϕ_{20}. Thus, we assume that:

$$\left.\begin{aligned}&a_1 = a_{11} + a_{10},\ a_2 = a_{21} + a_{20},\ \phi_1 = \phi_{11} + \phi_{10},\ \phi_2 = \phi_{21} + \phi_{20},\\ &\dot{a}_1 = \dot{a}_{11},\ \dot{a}_2 = \dot{a}_{21},\ \dot{\phi}_1 = \dot{\phi}_{11},\ \dot{\phi}_2 = \dot{\phi}_{21}.\end{aligned}\right\} \tag{38}$$

where $a_{10}, a_{20}, \phi_{10}$ and ϕ_{20} satisfy (28) and (31) and $a_{11}, a_{21}, \phi_{11}$ and ϕ_{21} are perturbations which are assumed to be small compared to $a_{10}, a_{20}, \phi_{10}$ and ϕ_{20} . Substituting (37) into (28)– (31), expanding for small $a_{11}, a_{21}, \phi_{11}$ and ϕ_{21} , and keeping linear terms in $a_{11}, a_{21}, \phi_{11}$ and ϕ_{21} , we get

$$\dot{a}_{11} = r_{11}a_{11} + r_{12}\phi_{11} + r_{13}a_{21} + r_{14}\phi_{21} \tag{39}$$

$$\dot{\phi}_{11} = r_{21}a_{11} + r_{22}\phi_{11} + r_{23}a_{21} + r_{24}\phi_{21} \tag{40}$$

$$\dot{a}_{21} = r_{31}a_{11} + r_{32}\phi_{11} + r_{33}a_{21} + r_{34}\phi_{21} \tag{41}$$

$$\dot{\phi}_{21} = r_{41}a_{11} + r_{42}\phi_{11} + r_{43}a_{21} + r_{44}\phi_{21} \tag{42}$$

where $r_{ij}, i = 1,2,3,4$ and $j = 1,2,3,4$ are provided in the Appendix.

Equations (39) to (42) can be presented in the resulting matrix:

$$\left[\dot{a}_{11}\ \dot{\phi}_{11}\ \dot{a}_{21}\ \dot{\phi}_{21}\right]^T = \left[J\right]\left[a_{11}\ \phi_{11}\ a_{21}\ \phi_{21}\right]^T \tag{43}$$

$$\left[J\right] = \begin{bmatrix} r_{11} & r_{12} & r_{13} & r_{14} \\ r_{21} & r_{22} & r_{23} & r_{24} \\ r_{31} & r_{32} & r_{33} & r_{34} \\ r_{41} & r_{42} & r_{43} & r_{44} \end{bmatrix} \tag{44}$$

$\left[J\right]$ is the Jacobian matrix.

Thus, the stability of the steady-state solutions depends on the eigenvalues of the Jacobian matrix. One can obtain the following eigenvalue equation:

$$\begin{vmatrix} r_{11}-\lambda & r_{12} & r_{13} & r_{14} \\ r_{21} & r_{22}-\lambda & r_{23} & r_{24} \\ r_{31} & r_{32} & r_{33}-\lambda & r_{34} \\ r_{41} & r_{42} & r_{43} & r_{44}-\lambda \end{vmatrix} = 0 \tag{45}$$

wherever the following polynomial's roots are located:

$$\lambda^4 + \Gamma_1\lambda^3 + \Gamma_2\lambda^2 + \Gamma_3\lambda + \Gamma_4 = 0 \tag{46}$$

The quantities of equation (45) $\left(\Gamma_i; i = 1,...,4\right)$ are pigeon-holed in the appendix. The Routh-Hurwitz criterion must be met for the solution to the abovementioned system to be stable, meaning that:

$$\Gamma_1 > 0, \Gamma_1\Gamma_2 - \Gamma_3 > 0, \Gamma_3(\Gamma_1\Gamma_2 - \Gamma_3) - \Gamma_1^2\Gamma_4 > 0, \Gamma_4 > 0 \tag{47}$$

3. Results and discussions

3.1. Time history performance without and with NVC controller

This study examines the stability of a forced, self-excited nonlinear beam system demonstrating the outer plate phenomenon. The system's behavior is analyzed numerically using the fourth-order Runge-Kutta method (implemented via MATLAB's ode45 function). Graphical representations of steady-state amplitudes versus detuning parameters illustrate the results σ_1, σ_2 , using defined system parameter values

$$(\gamma_1 = 0.1; \gamma_7 = 0.4; \gamma_8 = 0.5; b_1 = 0.1; b_7 = 0.7; b_8 = 0.8;\ f = 0.07; \alpha_2 = 1; \alpha_4 = 1; \omega_1 = \omega_2 = \Omega = 1.)$$

Figures 2 and 3 illustrate the steady-state amplitudes and Poincare maps of the system before and after implementing NVC controllers at the worst resonance case (approximately 0.4 and 0.4, respectively). The addition of NVC controllers significantly reduces the system amplitudes to 0.04 and 0.00013, respectively. This demonstrates the effectiveness of the NVC controllers. $E_{a.}$ =10, $E_{a.}$ =308, and vibrations are reduced by approximately 97.8% from their value without control

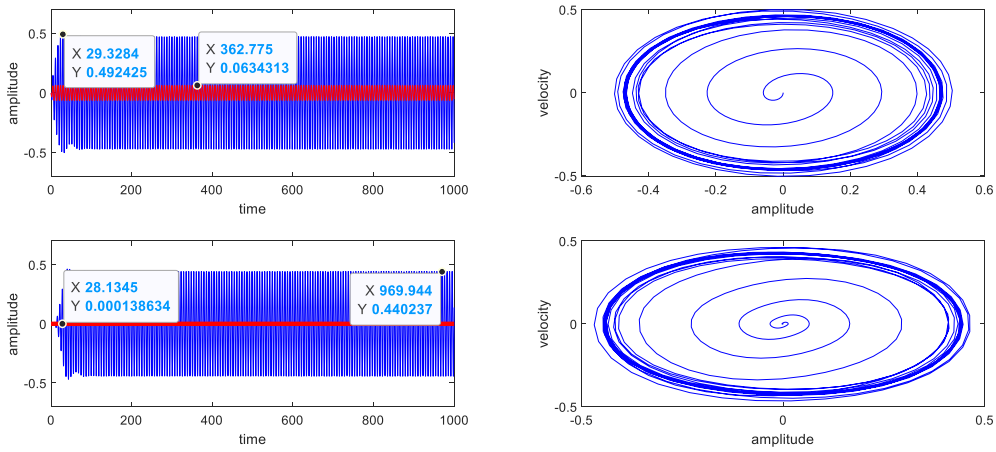

Figure 2. The amplitude of the focal system before and after adding the NVC controller.

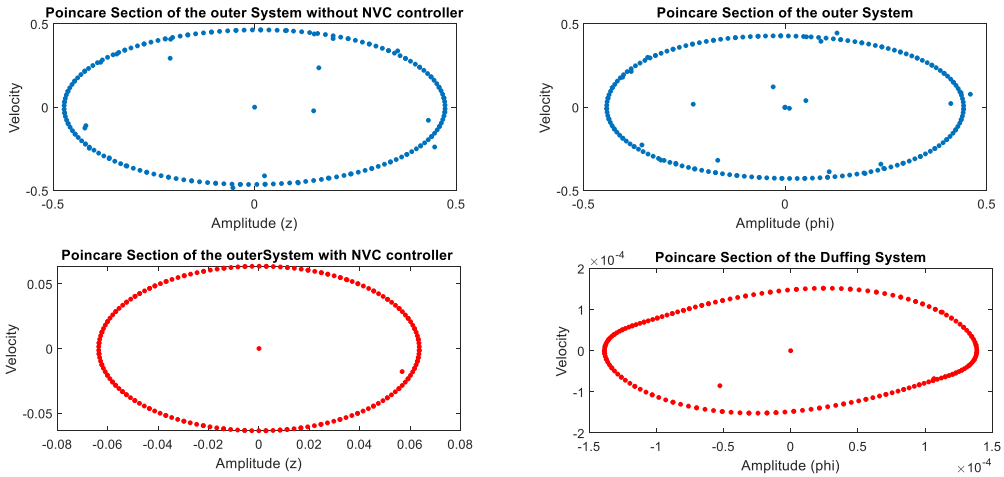

Figure 3. Poincare amplitude of outer plate system before and after adding the NVC controller.

3.2. Frequency Response curve (FRC)

The rejoinder's amplitude depends on both detuning parameters σ_1, σ_2 and excitation amplitude f . Solutions for system and NVC controller amplitudes are determined by solving equations numerically and graphically. The graphical solution, visualized against the detuning parameter σ_1, σ_2 , illustrates how system amplitudes change with detuning σ_1, σ_2 . Figures 4-14 show that frequency response curve amplitudes can be asymmetrical, but symmetry can be improved by parameter adjustment. Figure 4, depicting frequency response curves for the system with the NVC controller (stable solutions marked by solid lines), allows visual comparison of system responses across frequencies and highlights stability regions, showcasing the minimum primary system amplitude. Although the NVC controller mitigates vibrations under simultaneous resonance, controlled system amplitudes still rise with increasing harmonic excitation f . force. The resulting jump phenomenon leads to the main system's minimum achievable amplitude at $\sigma_1 = 0$, as shown in Figure 5. Figures 6 and 7 illustrate the impact of an NVC controller on system behavior under various conditions. Specifically, Figure 5 highlights the controller's ability to suppress vibrations even in the presence of simultaneous resonance, with the smallest primary system amplitude observed at $\sigma_1 = 0$. Furthermore, the data indicates that increasing the control gain α_2, α_4 leads to a further increased in system amplitude. This trend is evident in Figs 6 and 7, where a monotonic increase in amplitude is observed with increasing gain. Overall, the results presented in Figs 6-7 provide strong evidence for the efficiency of the NVC controller in mitigating system vibrations across a range of frequencies and operating conditions. Figs 8 and 9 illustrate the stimulus of the damping γ_1, b_1 on the system's vibration retort. The figures demonstrate that increasing the damping coefficient effectively reduces both the focal system's amplitude and the corresponding controller amplitude, particularly around the frequency. This suggests that the damping coefficient plays a significant role in the controller's ability to suppress vibrations. The data suggests that increasing the value of this nonlinear parameter corresponds to a decrease in overall amplitudes. This implies that the nonlinear parameter plays a role in mitigating system response, with higher values leading to greater suppression. Figs 10 and 11 demonstrate how changing the nonlinear parameter b_7, b_8 affects system amplitudes. The data shows that as the value of this nonlinear parameter increases, there's a corresponding increase in the overall amplitudes of the system. Fig 12 illustrates how the NVC controller behaves at low natural frequencies $\sigma_2 = 0$ i.e. ($\omega_1 = \omega_2$). The figure demonstrates that at these low frequencies, both the main system with NVC controller experiences an increase in peak amplitudes. However, despite this increase, the figure suggests that the NVC controller remains effective in this regime, indicating its suitability for systems with low natural frequencies. Fig. 13 further explores the controller's performance by examining three different values of the parameter you've indicated. The figure reveals that the focal structure's amplitude reaches its tiniest rate at what time this parameter is set to $\sigma_1 = \sigma_2$ .This finding highlights the NVC controller's enhanced efficiency in mitigating vibrations, particularly at resonance, where precise parameter tuning leads to optimal performance.

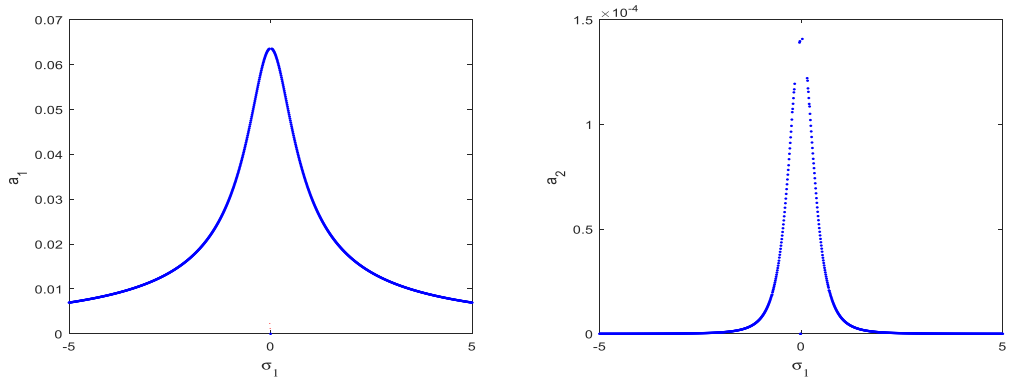

Figure 4**.** Resonance curves for system with NVC controller, respectively.

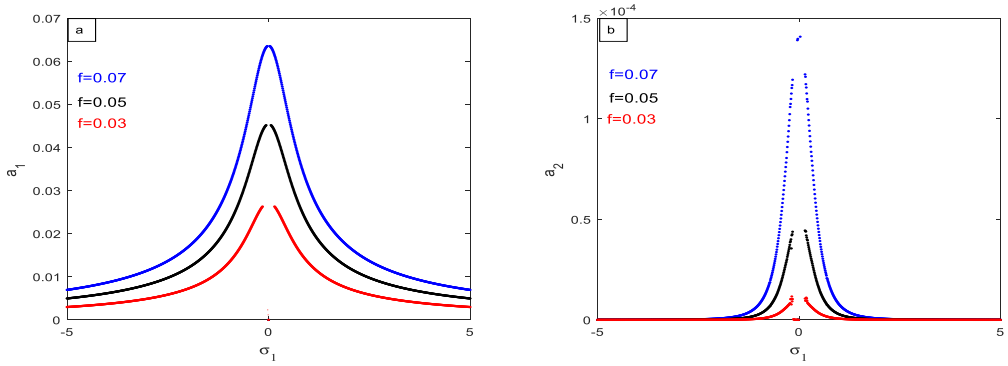

Figure 5. Frequency retort curve illustrating system amplitude variation across changed values of external force f on system with NVC controller.

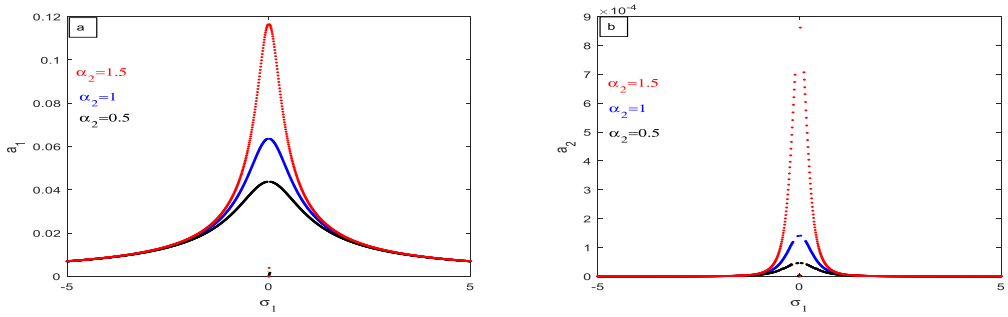

Figure 6. Frequency retort curve illustrating system amplitude variation across changed values of control signal gain α_2 on system with NVC controller.

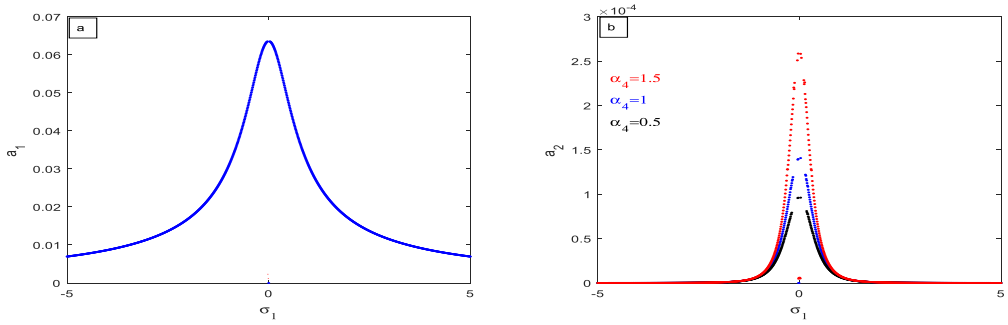

Figure 7. Frequency retort curve illustrating system amplitude variation across changed values of control signal gain α_4 on system with NVC controller.

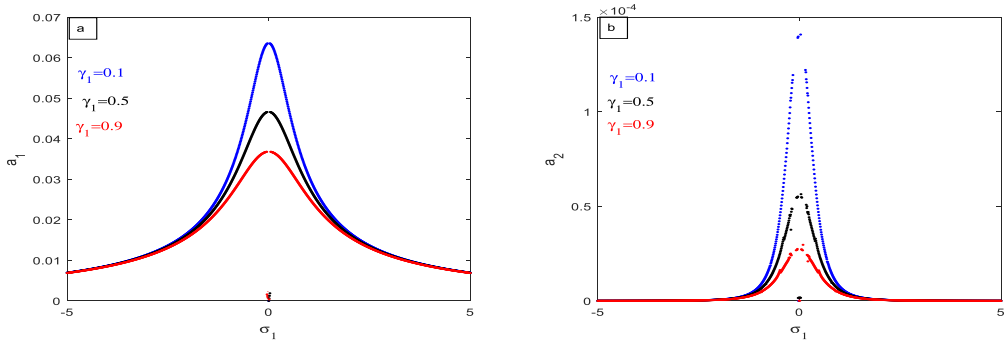

Figure 8. Frequency retort curve illustrating system amplitude variation across changed values of the damping coefficient γ_1 on system with NVC controller.

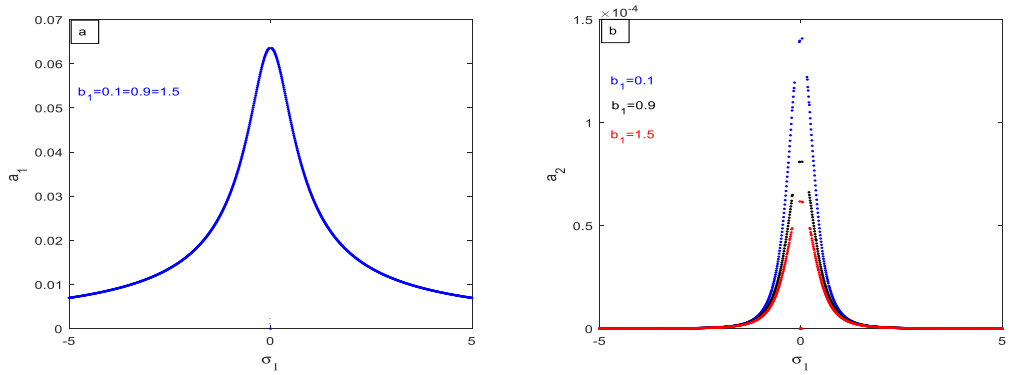

Figure 9. Frequency retort curve illustrating system amplitude variation across changed values of the damping coefficient b_1 on system with NVC controller.

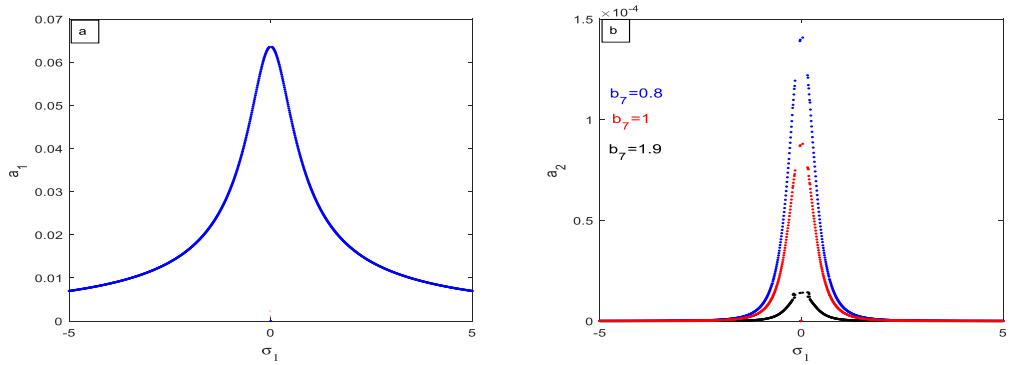

Figure 10. Frequency retort curve illustrating system amplitude variation across changed values of nonlinear parameter b_7 on system with NVC controller.

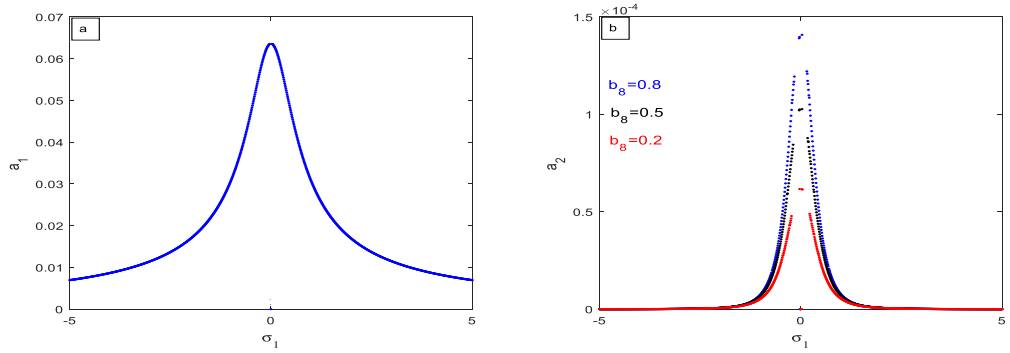

Figure 11. Frequency retort curve exemplifying system amplitude variation across changed values of nonlinear parameter b_8 on system with NVC controller.

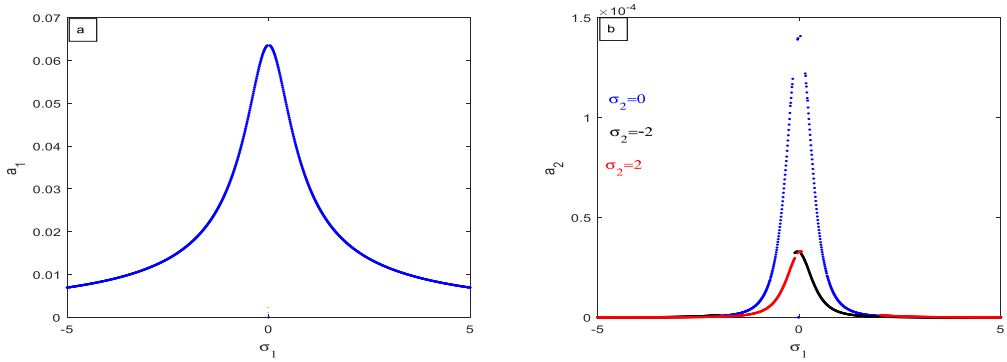

Figure 12. Result of changeable σ_2 on system with NVC controller.

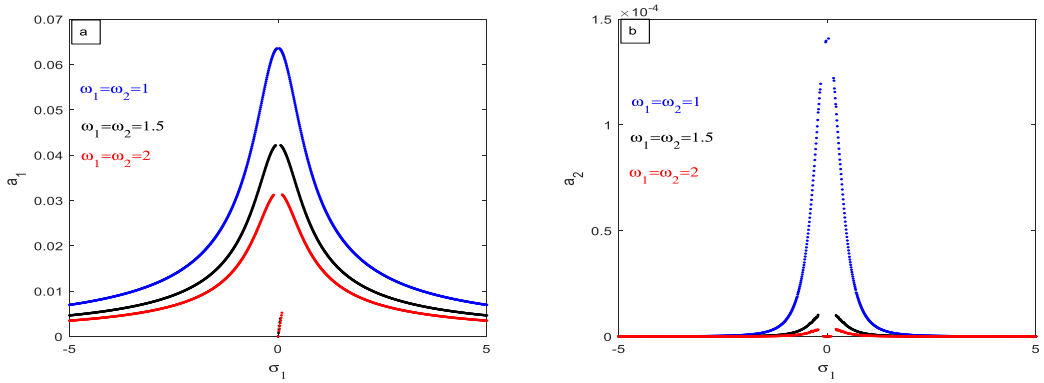

Figure 13. Outcome of changing $\omega_1 = \omega_2$ on system with NVC controller.

4. Assessment

4.1. Comparison between perturbation solution and numerical simulation.

Figures 14 and 15 demonstrate a strong correlation between numerical and approximate results for both uncontrolled and controlled systems (using a NVC controller). This close agreement validates the precision of both methods in representing the system's behavior across various control strategies, highlighting their robustness in analyzing system dynamics.

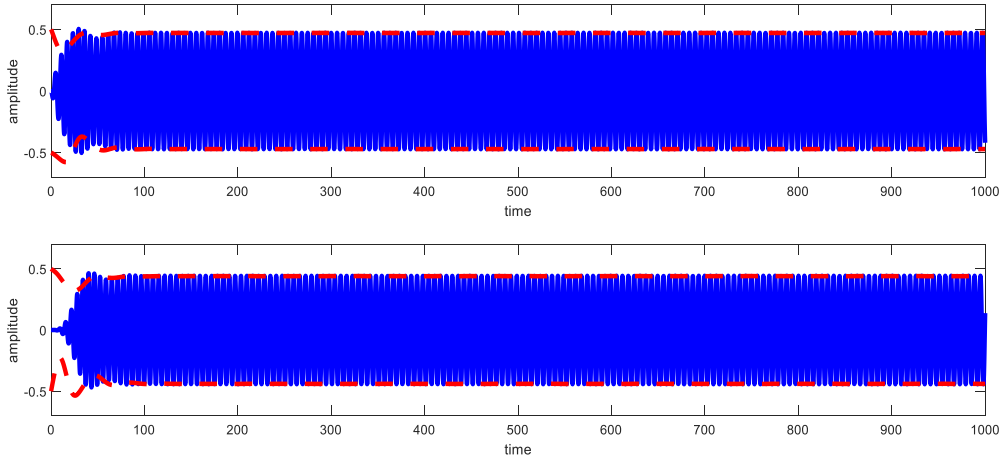

Figure 14. Vibration amplitude of uncontrolled main system.

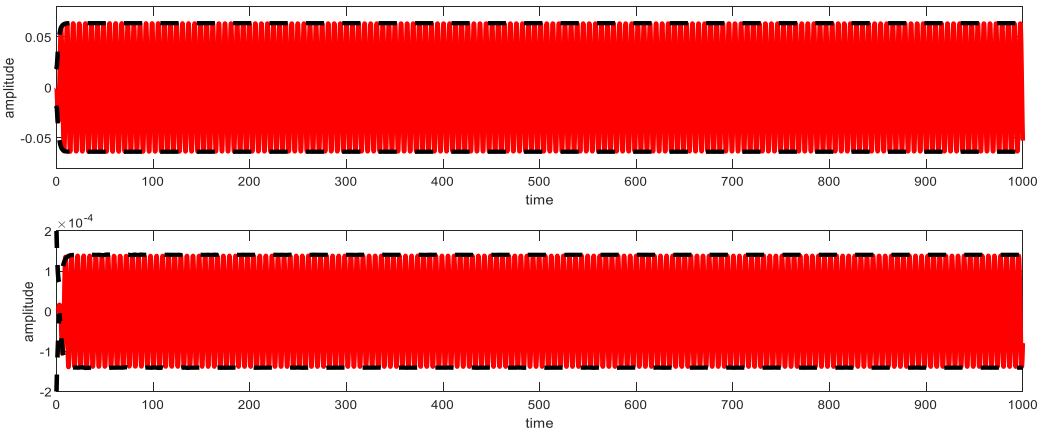

Figure 15. Contrast among the numerical solution(——)and approximate solution (……)

4.2. Assessment with previous work

Reference [7] Building upon the nonlinear vibration model of an axially moving wing aircraft presented in, which represents the aircraft wing as a stepped cantilever plate and considers aerodynamic forces, piezoelectric excitation, and in-plane excitation, this work introduces a PD controller. The model from is based on Reddy's higher-order shear deformation theory and Hamilton's principle, simplified using Galerkin's method. This paper Analysis of the system's time history and relevant parameters demonstrates the effectiveness of the implemented NVC controller in mitigating vibrations. Results show a substantial vibration amplitude reduction of approximately 97% with a control effort of nearly 10. A close correlation between numerical and approximate solutions validates the accuracy of the approach.

5. Conclusions

This study examines the vibration control of an "outer plate" in contact with another object, a scenario that generates complex nonlinear vibrations. The goal is to mitigate these vibrations, specifically lateral vibrations perpendicular to the plate's surface, using a negative velocity feedback controller. This controller generates a control signal based on the current error and its rate of change to actuate the system and dampen vibrations. The system's dynamics, including the controller's effect, are represented by coupled differential equations that capture the nonlinear plate behavior and the controller's interaction. Approximate solutions are obtained using a mathematical technique, and computer simulations solve these equations to model the system's behavior. Frequency response analysis is employed to understand the system dynamics and controller effectiveness. A sensitivity analysis explores the impact of parameter variations on performance to optimize the controller. Stability is assessed to prevent uncontrolled oscillations. Numerical simulations validate the analytical findings and demonstrate the control strategy's effectiveness, as shown by improved symmetry in frequency response amplitudes after parameter tuning. In summary, the key findings of this study are as follows:

- The NVC controller demonstrates high efficacy in regulating the system, achieving an effectiveness of approximately 10.
- The effervescent system's amplitude diminished by roughly 97% afterward implementing the NVC controller, related to its uncontrolled amplitude.
- The PR and IR case $\Omega \cong \omega_1$ & $\omega_2 = \omega_1$ is one of the worst vibrating resonance cases.
- Steady-state amplitude increased with excitation force f .
- Amplitude was contrariwise relative to both the damping factor γ_1, b_1 and the normal frequency ω_1, ω_2 .
- Increasing the gain of the NVC controller α_2, α_4 counterintuitively reduced it, a valuable finding for NVC controller implementation.
- Figures 16-17 demonstrate strong agreement between analytical and numerical solutions.
- NVC controller effectively mitigates high-amplitude vibrations within nonlinear systems.
- The minimum amplitudes of vibration in a suspended cable occur when $\sigma_1 = \sigma_2$.
- Frequency response curves derived using (FRC) solutions closely match those calculated using the 4th order Runge-Kutta method.
- The closed-loop response of the relative displacement, controlled by a NVC controller, exhibits a peak overshoot.
- A modified NVC controller effectively controlled the suspension system's relative displacement, minimizing peak overshoot and settling time.

Appendix

$$r_{11}=-\frac{1}{2}\gamma_1-\frac{1}{2}\alpha_2, r_{12}=\frac{f}{2\omega_1}\cos(\phi_{10}), r_{13}=\frac{-9\gamma_8}{8\omega_1}a_{20}{}^2\sin(\phi_{20}), r_{14}=\frac{-3\gamma_8}{8\omega_1}a_{20}{}^3\cos(\phi_{20}) \quad ,$$

$$r_{21}=\frac{\sigma_1}{a_{10}}-\frac{9\gamma_7}{8\omega_1}a_{10}, r_{22}=-\frac{f}{2\omega_1 a_{10}}\sin(\phi_{10}) \quad , \quad r_{23}=\frac{-9\gamma_8 a_{20}{}^2}{8\omega_1 a_{10}}\cos(\phi_{20}), r_{24}=\frac{3\gamma_8 a_{20}{}^3}{8\omega_1 a_{10}}\sin(\phi_{20}), r_{31}=\frac{9b_8 a_{10}{}^2}{8\omega_2}\sin(\phi_{20}) \quad ,$$

$$r_{32}=0, r_{33}=-\frac{1}{2}b_1-\frac{1}{2}\alpha_4, r_{34}=\frac{3b_8}{8\omega_2}a_{10}{}^3\cos(\phi_{20}) \quad , \quad r_{41}=\frac{9b_8 a_{10}{}^2}{8\omega_2 a_{20}}\cos\phi_{20}+\frac{\sigma_1}{a_{10}}-\frac{9\gamma_7}{8\omega_1}a_{10}, r_{42}=-\frac{f}{2\omega_1 a_{10}}\sin(\phi_{10}) \quad ,$$

$$r_{43}=\frac{\sigma_2-\sigma_1}{a_{20}}+\frac{9b_7 a_{20}}{8\omega_2}-\frac{9\gamma_8 a_{20}{}^2}{8\omega_1 a_{10}}\cos(\phi_{20}), \; r_{44}=-\frac{3b_8 a_{10}{}^3}{8\omega_2 a_{20}}\sin(\phi_{20})+\frac{3\gamma_8 a_{20}{}^3}{8\omega_1 a_{10}}\sin(\phi_{20})$$

$$\Gamma_1=-(r_{11}+r_{22}+r_{33}+r_{44}) \quad , \quad \Gamma_2=r_{22}(r_{11}+r_{33}+r_{44})+r_{44}(r_{11}+r_{33})+r_{11}r_{33}-r_{12}r_{21}-r_{13}r_{31}-r_{14}r_{41}-r_{24}r_{42}-r_{34}r_{43} \quad ,$$

$$\begin{aligned}\Gamma_3=&\, r_{11}(r_{24}r_{42}+r_{34}r_{43}-r_{22}(r_{33}+r_{44})-r_{33}r_{44})+r_{22}(r_{13}r_{31}+r_{14}r_{41}-r_{33}r_{44}+r_{34}r_{43})\\&+r_{33}(r_{12}r_{21}+r_{14}r_{41}+r_{24}r_{42})+r_{44}(r_{12}r_{21}+r_{13}r_{31})+r_{12}(r_{23}r_{31}+r_{24}r_{41})\\&+r_{14}(r_{21}r_{42}+r_{31}r_{43})+r_{34}(r_{13}r_{41}+r_{23}r_{42})\end{aligned} \quad ,$$

$$\begin{aligned}\Gamma_4=&\, r_{11}(r_{22}(r_{33}r_{44}-r_{34}r_{43})-r_{42}(r_{24}r_{33}+r_{23}r_{34}))-r_{22}(r_{41}(r_{14}r_{33}+r_{13}r_{34})+r_{31}(r_{13}r_{44}+r_{14}r_{43}))\\&-r_{33}(r_{12}(r_{21}r_{44}+r_{24}r_{41})+r_{14}r_{21}r_{42})-r_{12}(r_{31}(r_{23}r_{44}+r_{24}r_{43})-r_{34}(r_{21}r_{43}-r_{23}r_{41}))\\&+r_{42}(r_{31}(r_{13}r_{24}-r_{14}r_{23})-r_{13}r_{21}r_{34})\end{aligned}$$

References

1. Zhang, W., Chen, L. L., Guo, X. Y., & Sun, L. Nonlinear dynamical behaviors of deploying wings in subsonic air flow. Journal of Fluids and Structures, (2017), 74, 340-355.
2. Sanders, B., Crowe, R., & Garcia, E. Defense advanced research projects agency–smart materials and structures demonstration program overview. Journal of Intelligent Material Systems and Structures, (2004),15(4), 227-233.
3. Lu, S. F., Xue, N., Zhang, W., Song, X. J., & Ma, W. S. Dynamic stability of axially moving graphene reinforced laminated composite plate under constant and varied velocities. Thin-Walled Structures, (2021),167, 108176.
4. Wang, Y. H., & Qing, G. H. Analysis of piezoelectric composite laminates based on generalized mixed finite element. Acta Mater. Compos. Sin, (2022), 39(06), 2987-2996.
5. Zhang, W., Gao, Y. H., & Lu, S. F. Theoretical, numerical and experimental researches on time-varying dynamics of telescopic wing. Journal of Sound and Vibration, (2022), 522, 116724.
6. Liu, Y. Nonlinear dynamic analysis of an axially moving composite laminated cantilever beam. Journal of Vibration Engineering & Technologies, (2023), 11(7), 3307-3319.
7. Liu, Y., & Ma, W. Nonlinear Oscillations of a Composite Stepped Piezoelectric Cantilever Plate with Aerodynamic Force and External Excitation. Mathematics, (2023), 11(13), 3034.
8. Saeed, N. A., El-Ganini, W. A., & Eissa, M. Nonlinear time delay saturation-based controller for suppression of nonlinear beam vibrations. Applied Mathematical Modelling, (2013),37(20-21), 8846-8864.
9. Li, W., & Laima, S. Experimental Investigations on Nonlinear Flutter Behaviors of a Bridge Deck with Different Leading and Trailing Edges. Applied Sciences, (2020), 10(21), 7781.
10. Amer, Y. A., Abd EL-Salam, M. N., & EL-Sayed, M. A. Behavior of a Hybrid Rayleigh-Van der Pol-Duffing Oscillator with a PD Controller. Journal of applied research and technology (2022), 20(1), 58-67
11. Hamed, Y. S., Aly, A. A., Saleh, B., Alogla, A. F., Aljuaid, A. M., & Alharthi, M. M. Vibration performance, stability and energy transfer of wind turbine tower via PD controller. Computers, Materials & Continua, (2020),64(2), 871-886.
12. Bauomy, H. S., & El-Sayed, A. T. Act of nonlinear proportional derivative controller for MFC laminated shell. Physica Scripta, (2020), 95(9), 095210.
13. Ren, Y., & Ma, W. Dynamic Analysis and PD Control in a 12-Pole Active Magnetic Bearing System. Mathematics, (2024),12(15), 2331.
14. Omidi, E., & Nima Mahmoodi, S. Multimode modified positive position feedback to control a collocated struc-ture. Journal of Dynamic Systems, Measurement, and Control 2015, 137(5), 051003.

15. Bauomy, H. S., & El-Sayed, A. T. Outcome of special vibration controller techniques linked to a cracked beam. Appl. Math. Model 2018, 37, 266–287.
16. Jun, L. Positive position feedback control for high-amplitude vibration of a flexible beam to a principal resonance excitation. Shock and Vibration 2010, 17(2), 187-203.
17. Abdelhafez, H., & Nassar, M. Suppression of vibrations of a forced and self-excited nonlinear beam by using positive position feedback controller PPF. British Journal of Mathematics & Computer Science 2016, 17(4), 1-19.
18. Zhu, Q., Yue, J. Z., Liu, W. Q., Wang, X. D., Chen, J., & Hu, G. D. Active vibration control for piezoelectricity cantilever beam: an adaptive feedforward control method. smart materials and structures 2017, 26(4), 047003.
19. Alluhydan, K., Amer, Y. A., EL-Sayed, A. T., & EL-Sayed, M. A. Controlling the Generator in a Series of Hybrid Electric Vehicles Using a Positive Position Feedback Controller. Applied Sciences, (2024), 14(16), 7215.
20. Alluhydan, K., Amer, Y. A., EL-Sayed, A. T., & EL-Sayed, M. A. The Impact of the Nonlinear Integral Positive Position Feedback (NIPPF) Controller on the Forced and Self-Excited Nonlinear Beam Flutter Phenomenon. Symmetry, (2024). 16(9), 1143.
21. Das, A. S., Dutt, J. K., & Ray, K. Active control of coupled flexural-torsional vibration in a flexible rotor–bearing sys-tem using electromagnetic actuator. International Journal of Non-Linear Mechanics 2011, 46(9), 1093-1109.
22. El-Ganaini, W. A., Saeed, N. A., & Eissa, M. Positive position feedback (PPF) controller for suppression of nonlinear system vibration. Nonlinear Dynamics 2013, 72, 517-537.
23. Saeed, N. A., Awrejcewicz, J., Elashmawey, R. A., El-Ganaini, W. A., Hou, L., & Sharaf, M. On 1 2-DOF active damp-ers to suppress multistability vibration of a 2-DOF rotor model subjected to simultaneous multiparametric and ex-ternal harmonic excitations. Nonlinear Dynamics, (2024) ,1-34.
24. Fyrillas, M. M., & Szeri, A. J. Control of ultra-and subharmonic resonances. Journal of Nonlinear Science 1998, 8, 131-159.
25. Fischer, A., & Eberhard, P. Controlling vibrations of a cutting process using predictive control. Computational Me-chanics 2014, 54, 21-31.
26. Alluhydan, K., Moatimid, G. M., Amer, T. S., & Galal, A. A. Inspection of a Time-Delayed Excited Damping Duffing Oscillator. Axioms, (2024),13(6), 416.
27. Abdelhafez, H., & Nassar, M. Suppression of vibrations of a forced and self-excited nonlinear beam by using positive position feedback controller PPF. British Journal of Mathematics & Computer Science 2016, 17(4), 1-19.
28. Kandil, A., Hamed, Y. S., & Alsharif, A. M. Rotor active magnetic bearings system control via a tuned nonlinear sat-uration oscillator. IEEE Access, (2021), 9, 133694-133709.
29. Bauomy, H. (2023). Safety action over oscillations of a beam excited by moving load via a new active vibration con-troller. Mathematical Biosciences and Engineering: MBE, 20(3), 5135-5158.
30. Saeed, N. A., Awrejcewicz, J., Hafez, S. T., Hou, L., & Aboudaif, M. K. Stability, bifurcation, and vibration con-trol of a discontinuous nonlinear rotor model under rub-impact effect. Nonlinear Dynamics, (2023),111(22), 20661-20697.
31. Elashmawey, R. A., Saeed, N. A., Elganini, W. A., & Sharaf, M. An asymmetric rotor model under external, paramet-ric, and mixed excitations: Nonlinear bifurcation, active control, and rub-impact effect. Journal of Low Frequency Noise, Vibration and Active Control, (2024),14613484241259315.
32. Jamshidi, R., & Collette, C. Optimal negative derivative feedback controller design for collocated systems based on H2 and H∞ method. Mechanical Systems and Signal Processing, 2022,181, 109497.
33. Hamed, Y. S., Alotaibi, H., & El-Zahar, E. R. Nonlinear vibrations analysis and dynamic responses of a vertical con-veyor system controlled by a proportional derivative controller. IEEE Access 2020, 8, 119082-119093.
34. Amer, Y. A., & Abd EL-Salam, M. N. Negative Derivative Feedback Controller for Repressing Vibrations of the Hybrid Rayleigh-Van der Pol-Duffing Oscillator. Nonlinear Phenomena in Complex Systems 2022, 25(3), 217-228.
35. Kevorkian, J., Cole, J. D., Kevorkian, J., & Cole, J. D. The method of multiple scales for ordinary differential equations. Multiple Scale and Singular Perturbation Methods, 1996, 267-409.
36. Nayfeh, A. Perturbation Methods. New York: Wiley. 1973.
37. Dukkipati, R. V. Solving vibration analysis problems using matlab, New Age International Pvt Ltd Publishers. 2007.